Journal of Hazardous Materials 190 (2011) 416–423

Contents lists available at ScienceDirect

Journal of Hazardous Materials

journal homepage: www.elsevier.com/locate/jhazmat

Adsorption and degradation of model volatile organic compounds by a combined titania–montmorillonite–silica photocatalyst

Jiangyao Chen[a,b], Guiying Li[a], Zhigui He[a,b], Taicheng An[a,*]

[a] State Key Laboratory of Organic Geochemistry, Guangdong Key Laboratory of Environmental Resources Utilization and Protection, Guangzhou Institute of Geochemistry, Chinese Academy of Sciences, Guangzhou 510640, China
[b] Graduate School of Chinese Academy of Sciences, Beijing 100049, China

ARTICLE INFO

Article history:
Received 10 December 2010
Received in revised form 23 February 2011
Accepted 16 March 2011
Available online 27 March 2011

Keywords:
TiO_2 pillared montmorillonite
Immobilized photocatalyst
Adsorption
Photocatalytic degradation
Volatile organic compounds

ABSTRACT

A series of adsorptive photocatalysts, combined titania–montmorillonite–silica were synthesized. The resultant photocatalysts consisted of more and more spherically agglomerated TiO_2 particles with increasing of TiO_2 content, and anatase was the only crystalline phase with nano-scale TiO_2 particles. With increasing of the cation exchange capacity to TiO_2 molar ratio, specific surface area and pore volume increased very slightly. In a fluidized bed photocatalytic reactor by choosing toluene, ethyl acetate and ethanethiol as model pollutants, all catalysts had relatively high adsorption capacities and preferred to adsorb higher polarity pollutants. Langmuir isotherm model better described equilibrium data compared to Freundlich model. Competitive adsorptions were observed for the mixed pollutants on the catalysts, leading to decrease adsorption capacity for each pollutant. The combined titania–montmorillonite–silica photocatalyst exhibited excellent photocatalytic removal ability to model pollutants of various components. Almost 100% of degradation efficiency was achieved within 120 min for each pollutant with about 500 ppb initial concentration, though the efficiencies of multi-component compounds slightly decreased. All photocatalytic reactions followed the Langmuir–Hinshelwood model. Degradation rate constants of multi-component systems were lower than those for single systems, following the order of toluene < ethyl acetate < ethanethiol, and increased with the increase of adsorption capacities for different pollutants of various components.

1. Introduction

Volatile organic compounds (VOCs) mainly emitted from industrial processes and transport vehicles bring various environmental problems and have adverse effects on human beings. Kinds of physical, chemical and biological techniques have been utilized to remove them from air [1–3]. Among these different end-of-pipe abatement techniques, activated carbon adsorption is the most widely used. However, it just transfers organics from gas to solid phase. Comparatively, photocatalysis is an attractive technology for the removal of VOCs because it can completely mineralize these pollutants into CO_2 and H_2O without selection [4]. Hence, various photocatalysts such as metal oxides and chalcogenides have been developed [4–7]. While TiO_2 has been considered as the dominant photocatalyst due to its properties of superior photocatalytic oxidation ability, nonphotocorrosive, nontoxic, and inexpensive characteristics [8]. Unfortunately, the concentration of pollutants in ambient water and air is quite low and the adsorption of pollutants onto the TiO_2 photocatalyst is often limited due to its small specific surface area, leading to very low photocatalytic degradation efficiency. A possible way to overcome this is to add a co-adsorbent to the TiO_2 photocatalyst to combine high adsorptive ability of co-adsorbent with high photocatalytic activity of TiO_2 [9,10].

Clays have been investigated as a new class of composite materials during past few decades. Many organic [11,12] or inorganic cations [13,14] are intercalated into the silicate layers of clays to synthesize diversified pillared materials. Of them, extensive concern has been focused on the TiO_2 pillared clay which can be applied to adsorb various organics from water and air [15–18]. Nevertheless, photocatalytic activity of TiO_2 pillared clay is still not high enough due to its low adsorption capacity [19,20]. As known, photocatalytic oxidation occurs on the catalyst surface where the adsorption of the pollutants is essential process [21]. To increase the adsorption capacity of the TiO_2 pillared clay, the immobilization of TiO_2 pillared clay on porous materials may be a practicable method. Silica gel has attracted considerable interest as an excellent support since it is transparent to near-UV light, has large specific surface area and strong adsorbability [5]. In addition, the adsorption and condensation properties of the supports greatly depend on their surface hydrophilic–hydrophobic properties [22]. TiO_2 pil-

* Corresponding author. Tel.: +86 20 85291501; fax: +86 20 85290706.
E-mail address: antc99@gig.ac.cn (T. An).

0304-3894/$ – see front matter © 2011 Elsevier B.V. All rights reserved.
doi:10.1016/j.jhazmat.2011.03.064

lared clay prefers to enrich and photocatalytically degrade organics with high hydrophobicity in water and air due to its hydrophobic interlayer surface [23,24]. While the surface of SiO_2 exhibits hydrophilic nature originated from the surface hydroxyl groups [25]. Therefore, by controlling the mass ratio of TiO_2 pillared clay and silica gel, photocatalysts with different selective ability to abate different polarity VOCs in air can be prepared. However, to date, such photocatalysts have not been reported yet. Furthermore, VOCs always exist as a mixture of many species rather than single component in practical case. Unfortunately, very few publications to date have investigated the relationship between the competitive adsorption and the photocatalytic process in the presence of multiple VOCs.

In present work, by initially intercalated TiO_2 into the montmorillonite and then immobilized onto the silica gel, a series of adsorptive photocatalysts were synthesized to remove low-level concentration VOCs from air. Toluene is a toxic compound listed in Title III of the 1990 Clean Air Act Amendment proposed by the Environmental Protection Agency of USA; ethyl acetate (EA) is a kind of irritative and explosive compound with fragrant odor [2], which is harmful to respiratory systems of mankind [26], while ethanethiol (EtSH) is high toxic pollutants with strong unpleasant odor and very low perceptibility threshold [27]. Three VOCs with different polarities as single and multinary VOCs were chosen as the model pollutants in a fluidized bed photocatalytic reactor to evaluate the adsorptive performance and photocatalytic activity of the prepared photocatalysts. Langmuir and Freundlich isothermal models were used to fit the isothermal adsorption data and the Langmuir–Hinshelwood (L–H) equation was applied to model the photocatalytic degradation reactions.

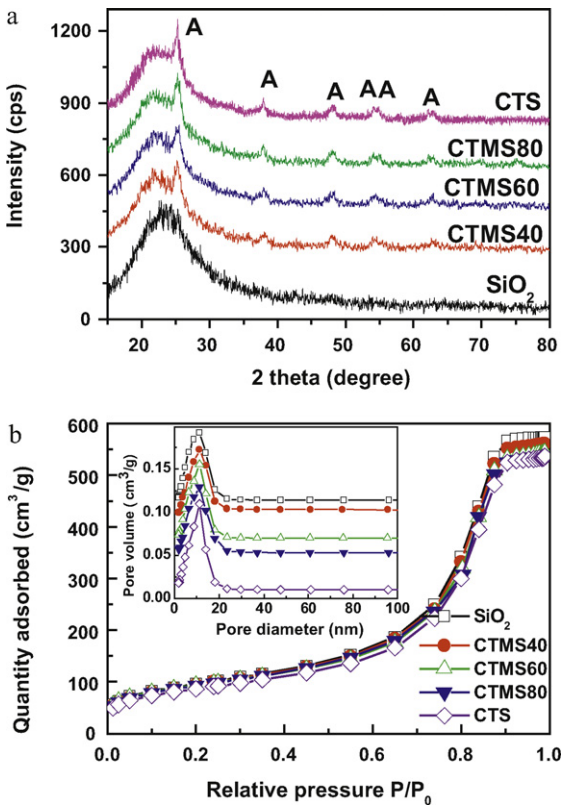

Fig. 1. (a) XRD diffraction patterns (A: TiO_2 anatase); (b) N_2 adsorption isotherms and pore size distribution curves of the prepared photocatalysts and pretreated SiO_2.

2. Materials and methods

2.1. Materials and reagents

Silica gel (150–180 μm) was purchased from Qingdao Haiyang Chem. Co., Ltd., China. Toluene, EA and EtSH were all analytical grades from Tianjin Chemical Reagent Co., Inc., China. Tetra-n-butyl titanium (Ti $(OC_4H_9)_4$) and glacial acetic acid were from Shanghai Chemical Reagent Co., Inc., China. Sodium montmorillonite was prepared in our laboratory method with montmorillonite from Lin'an, Zhejiang, China [28]. Certain silica gel was immersed into 0.35 mol/L nitric acid solution for 1 h and then washed with deionized water for several times until the pH value is around 7.0, and the wet silica gel was dried at 100 °C before use.

2.2. Preparation and characterization of photocatalysts

For a typical synthesis, 15 g of Ti $(OC_4H_9)_4$ was added drop-by-drop to 90 ml of acetic acid solution under vigorous stirring. After being sealed and stirred for 3 h, the obtained clear TiO_2 sol was added to 1 wt% of sodium montmorillonite suspension slowly with the molar ratio of cation exchange capacity (CEC)/TiO_2 was 1/40 (60 or 80). Stirring was continued for another 24 h at room temperature before 50 g of pretreated silica gel was added. The final mixture was stirred for 2 h, dried at 120 °C for 24 h and then calcinated at 450 °C for 4 h to obtain the combined titania–montmorillonite–silica labeled as CTMS40, CTMS60 and CTMS80, respectively. The photocatalyst, combined titania–silica (CTS), was prepared by the same process as preparing CTMS40 but without adding montmorillonite. The TiO_2 content in this work was about 7 wt% of the silica gel.

A Rigaku Dmax X-ray diffractometer (XRD) with Cu Kα radiation was used to record the patterns of the prepared photocatalysts and pretreated silica gel. Nitrogen adsorption data were obtained by using a micromeritics Gemini V surface area and pore analyzer while the morphology was studied using scanning electron microscope (SEM, SU-1500).

2.3. Adsorption and photocatalytic degradation experiments

Experimental equipment used consists a gas sample reservoir (15 L), a gas circulation pump, a switch, a flow meter, an injection-sampling port, a Teflon tubing, and a fluidized bed photocatalytic reactor within which a 125 W high-pressure mercury lamp with a maximum emitting radiation of 365 nm (GGZ125, Shanghai Yaming Lighting Co., Ltd.) as the UV-light source was installed (a detailed description of the reactor is given in supporting information) [5]. Isothermal adsorption experiments of toluene, EA and EtSH on these prepared photocatalysts and the pretreated silica gel were investigated with the initial concentrations varying from 5 to 90 ppm. CTMS80 was chosen as a representative to evaluate the adsorption ability and photocatalytic activity of the prepared photocatalysts in the adsorption and photocatalytic degradation kinetics experiments. The adsorption experiments for single and mixed compounds on the photocatalyst were carried out with the initial concentration of about 1500 ppb for each pollutant. For photolysis and photocatalysis, the pollutants (initial concentration was about 500 ppb) were allowed to reach the gas–solid adsorption equilibrium before the lamp was switched on. Unless otherwise specified, all experiments were performed using 5 g of the prepared photocatalysts or the pretreated silica gel, and the circulation velocity of gas was maintained at 100 L/h. The concentrations of pollutants were analyzed by gas chromatography (GC-900A) equipped with a flame ionization detector. A detailed description of the pollutant analysis is given in supporting information.

Table 1
Structure parameters of the prepared photocatalysts and the pretreated silica gel.

Samples	CTS	CTMS80	CTMS60	CTMS40	SiO_2
Average pore size (nm)	10.07	10.85	10.68	10.55	10.48
BET[a] surface area (m^2/g)	293.8	306.0	310.9	319.4	338.5
BJH[b] total volume (cm^3/g)	0.8256	0.8298	0.8306	0.8331	0.8867

[a] Brunauer–Emmett–Teller.
[b] Barrett–Joyner–Halen.

3. Results and discussion

3.1. Characterization

The XRD patterns of the prepared photocatalysts and the pretreated silica gel are illustrated in Fig. 1a. Besides a broad characteristic peak of amorphous SiO_2, the XRD patterns obtained from samples CTMS40, CTMS60, CTMS80 and CTS exhibit similar characteristics, where anatase peaks are clearly found at $2\theta = 25.3^\circ$, 37.2°, 48.9°, 54.0°, 55.3° and 62.4°, suggesting that anatase is the only crystalline phase in samples [29]. In contrast, no characteristic peaks of the montmorillonite are discerned due to its low content in the CTMSs. In the case of CTMS40, CTMS60, CTMS80 and CTS, the mean crystallite sizes of TiO_2 particles are 10.0, 11.5, 11.0 and 12.2 nm, respectively, which are calculated from the broadening of the $2\theta = 25.3^\circ$ XRD peaks of anatase phase according to the Scherrer formula. It seems that the crystallite sizes of CTMS40, CTMS60 and CTMS80 are all nano-scale and smaller than that of CTS. This result confirms that pillaring TiO_2 particles into montmorillonite can further reduce the crystallite size of TiO_2 particles and smaller particles may lead to higher photocatalytic activity.

Fig. 1b shows the N_2 adsorption isotherms and pore size distribution curves of the prepared photocatalysts and pretreated silica gel. Similar characteristics were observed from all adsorption isotherms, which exhibit the same type IV adsorption shapes [30]. Close average pore sizes are also obtained for CTS (10.07 nm), CTMS80 (10.85 nm), CTMS60 (10.68 nm), CTMS40 (10.55 nm) and SiO_2 (10.48 nm) from the pore size distribution curves (inset in Fig. 1b). These results reveal that most of the pore channels of the support silica gel are available, whereas a small portion of the pores may be filled by TiO_2 or TiO_2 pillared montmorillonite particles, which can be further confirmed by the specific surface areas and pore volumes presented in Table 1. From CTS to pure SiO_2, the specific surface area and pore volume merely increase from 293.8 m^2/g and 0.8256 cm^3/g to 338.5 m^2/g and 0.8867 cm^3/g, respectively. For CTMSs, with the increase of the molar ratio of CEC to TiO_2, the specific surface area and pore volume increase, indicating that CTMS40 may possess the highest adsorption capability. The adsorptive

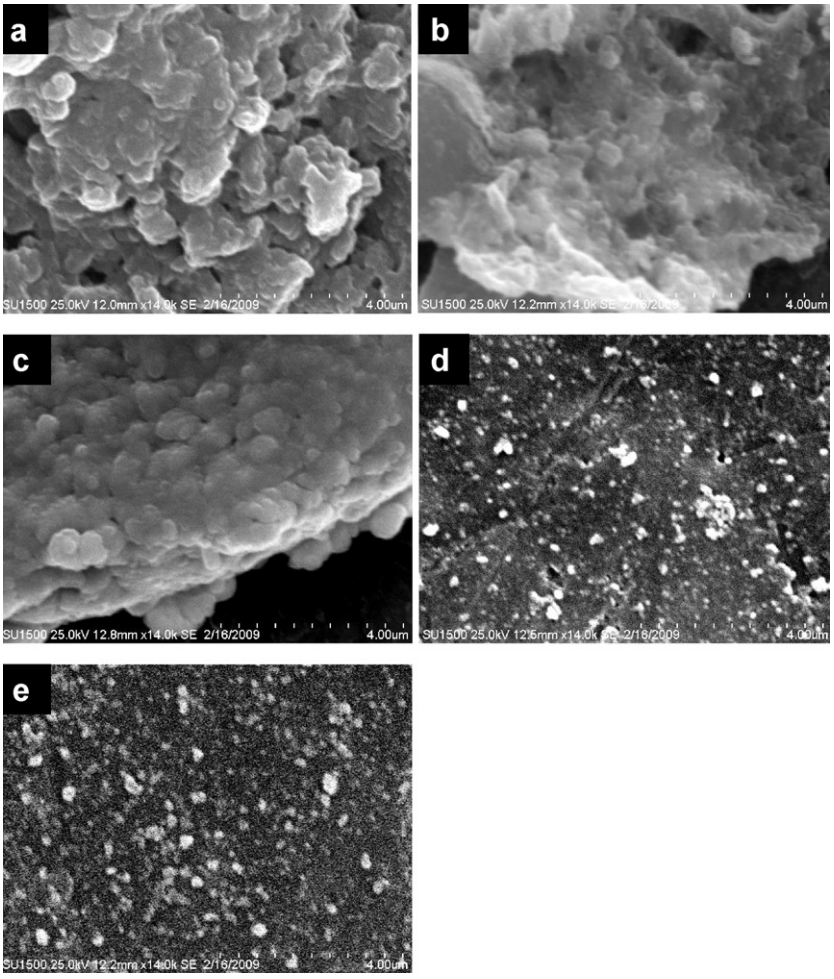

Fig. 2. SEM images of the prepared photocatalysts and pretreated SiO_2 ((a) CTMS40, (b) CTMS60, (c) CTMS80, (d) SiO_2, (e) CTS).

performance of the prepared samples may be very close but follow this order: CTS < CTMS80 < CTMS60 < CTMS40 < SiO_2. This hypothesis is adequately confirmed by the isothermal adsorption results discussed below.

SEM images of the prepared photocatalysts and the pretreated silica gel are displayed in Fig. 2. From CTMS40 (Fig. 2a) to CTMS60 (Fig. 2b) and to CTMS80 (Fig. 2c), as the content of TiO_2 increases, more and more spherically agglomerated TiO_2 particles are formed and clearly discerned, indicating that CTMS80 may possess the best photocatalytic activity. Also, less and less pore structures are observed from CTMS40 to CTMS80, suggesting that, with the increase of the molar ratio of TiO_2 to CEC, more pores of the silica gel will be plugged and the adsorption capability of the CTMSs may decrease, which is consistent with the results obtained from the isothermal adsorption experiments discussed below. The images of silica gel and CTS are also presented in Fig. 2d and e, respectively. Comparatively, after loading TiO_2 on the SiO_2, besides SiO_2 particles, lots of small TiO_2 particles are formed and distributed uniformly on the SiO_2 surface.

3.2. Isothermal adsorption

The isothermal adsorption curves of toluene on the prepared photocatalysts and pretreated silica gel are displayed in Fig. 3a. All of the prepared samples show relatively high adsorption capacities for toluene while a decrease trend is observed from SiO_2 to CTS, which is accordant with the relations of the specific surface areas and pore volumes for all samples. In the case of CTMSs, with the increase of molar ratio of TiO_2 to CEC, more TiO_2 particles will form outside the pillared montmorillonite (Fig. 2), plug more pores of the silica gel and then weaken the adsorption capability of the prepared photocatalysts. However, due to the relatively low TiO_2 content (about 7 wt% of the silica gel) in the CTMSs, the silica gel and CTMSs showing very close adsorption capacities suggest that this weakening is very slight. Moreover, it is obvious that the contribution of TiO_2 pillared montmorillonite particles to the adsorption capability is much greater than that of TiO_2 particles in this work by comparing the adsorption capacities of CTMS40 and CTS. Similar results can also be obtained from the adsorption isotherms of EA and EtSH (Fig. 3b and c).

As known, the isothermal adsorption model plays an important role in analyzing the procedure of adsorption systems and describing the equilibrium situation. The Langmuir (Eq. (1)) and Freundlich models (Eq. (2)) are the simplest and most useful models. In this work, both models are used to describe the data of adsorption isotherms and can be represented as follows [31,32]:

$$Q = \frac{Q_{max} bC}{1 + bC} \quad (1)$$

$$Q = KC^{1/n} \quad (2)$$

where Q (mg/g) and C (ppm) are the equilibrium adsorption capacity and the equilibrium concentration of adsorbate, respectively. Q_{max} (mg/g) is the theoretical maximum adsorption capacity and b (ppm^{-1}) is the energy of adsorption, both of which are Langmuir constants. While K and n are the Freundlich constants related to adsorption capacity and adsorption intensity of the adsorbent, respectively.

The theoretical Langmuir and Freundlich constants are listed in Table S1. For the adsorption of toluene on CTMS80, the experimental adsorption capacity Q (15.4 mg/g) (Fig. S1a) is smaller than the theoretical maximum adsorption capacity Q_{max} (20.9 mg/g) (Table S1) calculated by Eq. (1), indicating that toluene is adsorbed on CTMS80 by a monolayer type adsorption in which the surface of the prepared sample is not fully covered [33]. In the case of Freundlich constants, it has been reported that n value between 1 and 10 represents favorable adsorption [34]. In Table S1, the values of n are all higher than 1.89 and lower than 2.53, implying favorable adsorption for toluene by these prepared samples. Moreover, with the increase of K values, the adsorption intensity becomes greater. The highest and lowest K values were obtained for SiO_2 (3.40) and CTS (2.34), respectively, for the adsorption of toluene, confirming that the adsorption capacity of SiO_2 is greater than that of CTS to toluene. In addition, the adsorption of EA and EtSH on the same prepared samples are also investigated and it is found that Q_{max} and K values follow the order of toluene < EA < EtSH. All these theoretical calculations are consistent with the experimental results. Similar results can be also obtained from the adsorption of EA or EtSH. Furthermore, the correlation coefficients (R^2) are all beyond 0.958 which also means that both the Langmuir and Freundlich isotherm models well fit the adsorption experimental data while the Langmuir model shows the better goodness-of-fit ($R^2 \geq 0.997$).

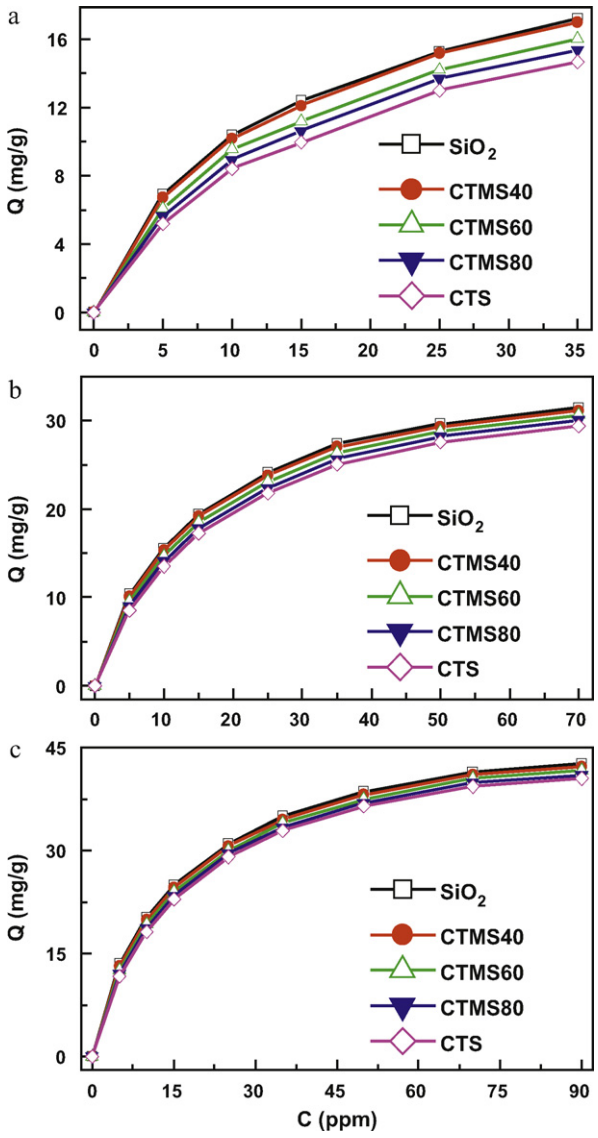

Fig. 3. Adsorption isotherms of toluene (a), EA (b) and EtSH (c) on the prepared photocatalysts and pretreated SiO_2.

As discussed, the adsorption capacity increases in the order of the adsorbates: toluene < EA < EtSH and this result may be attributed to the different affinities of adsorbates to the adsorbents. As it is generally accepted that the adsorbability of gaseous organics on the adsorbent relies on their physical properties [35].

Table 2
Adsorption capacities and photocatalytic degradation rate constants.

Different component			Adsorption capacity (mg/g)	Photocatalytic degradation rate constant (min^{-1})
Single component	Toluene		2.23	0.0338
	EA		3.41	0.0489
	EtSH		4.50	0.0577
Binary component	Toluene and EA	Toluene	0.82	0.0321
		EA	3.26	0.0380
	Toluene and EtSH	Toluene	0.74	0.0309
		EtSH	4.34	0.0553
	EA	EA	1.64	0.0323
	and EtSH	EtSH	4.09	0.0502
Ternary component	Toluene, EA and EtSH	Toluene	0.64	0.0230
		EA	1.53	0.0278
		EtSH	3.99	0.0361

Herein, four characteristic parameters of the adsorbates (molecular weight, boiling point, vapor pressure and dielectric constant), summarized in Table S2, are selected to evaluate the relations between them and the adsorption capacities on pretreated silica gel which is the dominant component for support in all prepared samples (Fig. S1). The adsorption capacities of all adsorbates increase with the decrease of the molecular weight (Fig. S1a) and boiling point (Fig. S1b) while the increase of the vapor pressure (Fig. S1c) and dielectric constant (Fig. S1d). All good correlations ($R^2 \geq 0.791$) between adsorption capacities and these characteristic parameters of adsorbates are obtained, and the highest correlation coefficient ($R^2 = 0.990$) between equilibrium adsorption capacity and dielectric constant is achieved, indicating that the pretreated silica gel prefers to adsorb pollutant with high dielectric constant, high vapor pressure, low boiling point and low molecular weight, while the dielectric constant should mainly contribute to the affinity of the model pollutants on the adsorbent surface. This conclusion is also suitable for our prepared all photocatalysts in this work (results not shown). It is also concluded that a good linear relation between dielectric constant and polarization existed in strongly polar media [36]. Moreover, the prepared photocatalysts in this work may possess polarity because the dominant component of all prepared photocatalysts is SiO_2, where silicon has polar nature [31]. Therefore, pollutants with higher polarity can be easier adsorbed and enriched on our prepared photocatalysts.

3.3. Adsorption kinetics of single and multiple VOCs on CTMS80

Based on the isothermal adsorption experiments, single-component adsorption kinetics of toluene, EA and EtSH on CTMS80 as an example of prepared photocatalysts are carried out in detail (Fig. S2). The adsorption capacities (Q) increase rapidly in the first 30 min and reach equilibrium within 60 min for all pollutants. After 90 min, for toluene, EA and EtSH, the adsorption capacities (Table 2) are 2.23, 3.41 and 4.50 mg/g, respectively. These results also confirm that the organic pollutant with higher polarity is easier to be adsorbed and enriched onto the photocatalysts prepared in present work.

Fig. 4 also shows the multi-component competitive adsorption kinetics of three model pollutants on CTMS80. Obviously, all model pollutants are adsorbed swiftly on the prepared photocatalyst at initial 15–20 min, competitive adsorption happens with an extended time. This phenomenon was also found for the mixed toluene and benzene by other researchers [37]. For binary-component adsorption between toluene and EA (Fig. 4a), the adsorption kinetics of toluene first decreases and then increases

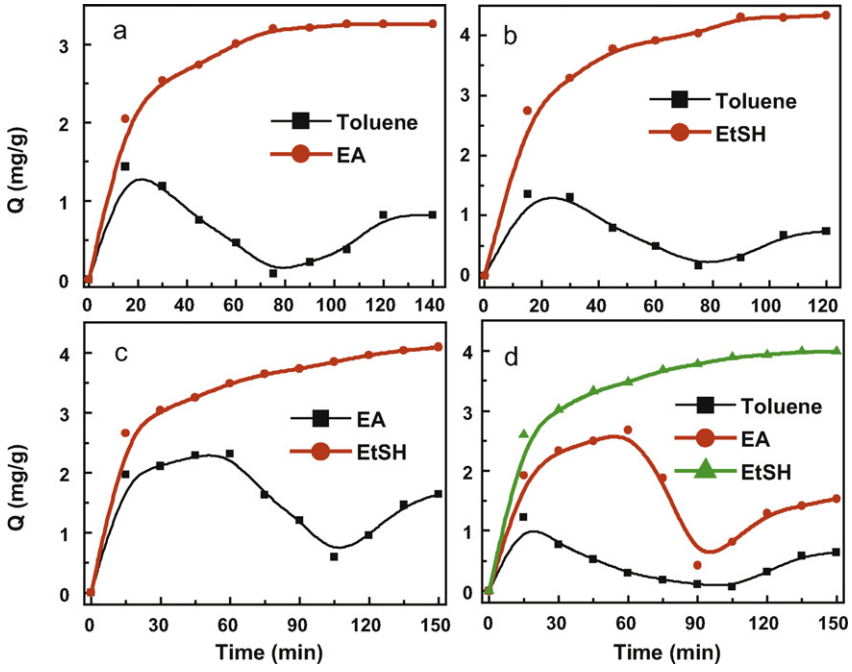

Fig. 4. Competitive adsorption of toluene with EA (a), toluene with EtSH (b), EA with EtSH (c) and toluene, EA with EtSH (d) onto CTMS80.

to reach equilibrium with time, while the adsorption of EA increases constantly. The result can be ascribed to the different adsorption affinity of each pollutant to CTMS80 which will be discussed later. Similar results can be observed in the binary-component adsorption of toluene with EtSH (Fig. 4b), EA with EtSH (Fig. 4c) and in the ternary-component adsorption (Fig. 4d). By comparison of the results in Figs. S2 and 4, the adsorption capabilities of toluene, EA and EtSH in single-component adsorption systems are all higher than those in the multi-component adsorption systems, which is a confirmation of the competitive adsorption.

To clearly see the effect of competitive adsorption on the adsorption efficiency, the adsorption capacities of toluene, EA and EtSH of various components are further investigated (Table 2). The adsorption capacities of all model pollutants decrease with the increase of the component of coexisting model pollutants. For toluene, the adsorption capacity for single-component adsorption (2.23 mg/g) is about three times higher than that of simultaneous adsorption of the mixtures (in the binary system, the adsorption capacity of toluene is 0.82 (with EA) and 0.74 mg/g (with EtSH) respectively, while in the ternary system, the adsorption capacity of toluene decreases to 0.64 mg/g). For EA, the adsorption capacity in single system (3.41 mg/g) is slightly higher than that for co-adsorption with toluene (3.26 mg/g), and more than twice as high as that for co-adsorption with EtSH (1.64 mg/g) or that for ternary-component adsorption (1.53 mg/g). Obviously, the adsorption capacity of EA for binary EA and EtSH is almost 50% as for binary EA and toluene. All these can be interpreted as follows: for multi-component adsorption, pollutants are synchronously adsorbed on the CTMS80 surfaces at the beginning of the adsorption. However, with the increase of the time, the pollutant with weaker polarity adsorbed on the surface of the CTMS80 may be competed and even displaced by the specie with stronger polarity, due to the polarity of CTMS80 as mentioned. In this work, the polarity of these model pollutants follows the order of toluene < EA < EtSH, therefore, toluene is competed or even displaced by EA or/and EtSH, while for binary EA and EtSH, EA is inhibited by EtSH, leading to relatively great disparities of adsorption capacities for toluene and EA. In the case of EtSH, because of its strongest affinity to the CTMS80, competitive adsorption shows smallest impact to the adsorbability of EtSH, although slight decrease is observed for the adsorption capacities for ternary-component adsorption (3.99 mg/g) compared with single-component adsorption (4.50 mg/g).

3.4. Photocatalytic degradation of VOCs on CTMS80

The photolysis of model pollutants without photocatalyst is first performed to explore the role of UV light in photocatalytic oxidation processes (Fig. 5a). Only less than or equal to 3% of the pollutants are photolyzed after 2 h irradiation, indicating that only UV light irradiation cannot effectively decompose these model pollutants. Meanwhile, the photolytic efficiencies of the pollutants obey the order of EA < toluene < EtSH.

As expected, in the presence of the photocatalyst CTMS80, the concentrations of three model pollutants decrease dramatically under UV illumination (Fig. 5b). The degradation efficiencies of them increase rapidly within first 60 min and reach more than 90% within 75 min. After 120 min, no more pollutants can be detected. It is indubitable that CTMS80 shows excellent photocatalytic activity to the model pollutants, especially to EtSH. By comparison, the removal efficiency of EA is higher than that of toluene in the presence of the photocatalyst, whereas the former is slightly lower than the latter during the photolytic procedures. As discussed, the affinity of EA to the prepared photocatalyst in this work is stronger than that of toluene. Therefore, in the presence of CTMS80, EA is more strongly adsorbed on the photocatalyst, leads to the better contact of photocatalyst-light and photocatalyst-reactant. In this case, higher photocatalytic oxidation efficiency of EA could be obtained.

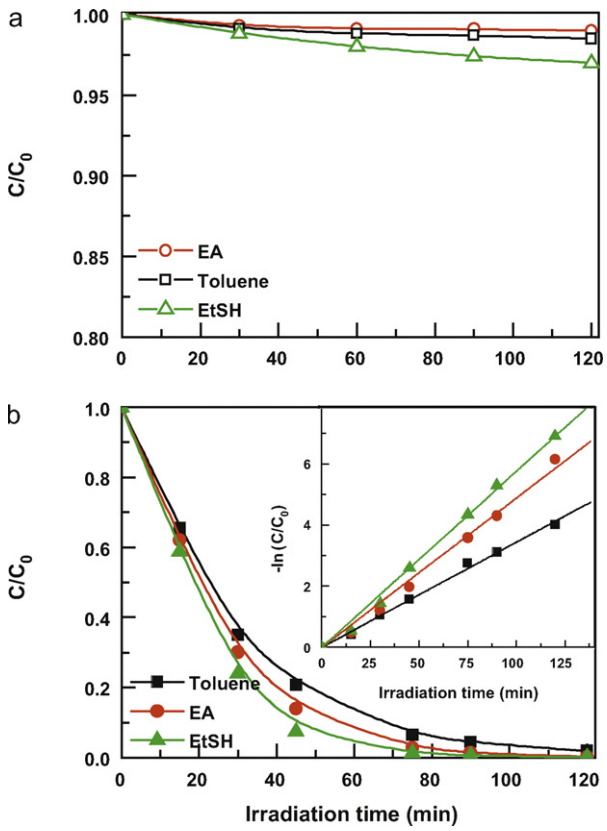

Fig. 5. Photolytic (a) and photocatalytic (b) degradation kinetics of toluene, EA and EtSH onto CTMS80.

As known, photocatalytic oxidation of VOCs conformed to L–H kinetics model [5,38] and the linear plots of $-\ln(C/C_0)$ versus irradiation time (inset in Fig. 5b) revealed that the photocatalytic degradation kinetics of single model pollutants on CTMS80 also matched the L–H model. The relevant reaction rate constants are calculated in Table 2 according to the equation: $-\ln(C/C_0) = kt$, where C_0 is the initial concentration of reactant and k is the rate constant. From the table, the photocatalytic degradation rate constants for single model pollutants follow the order of toluene ($0.0338\ \text{min}^{-1}$) < EA ($0.0489\ \text{min}^{-1}$) < EtSH ($0.0577\ \text{min}^{-1}$). Obviously, this reaction rate trend is consistent with the adsorption trend of the three VOCs onto the CTMS80.

Since competitive adsorption of mixed VOCs may lead to the decreases of the photocatalytic degradation efficiency and the rate constant of each compound, four sets of photocatalytic degradation experiments on CTMS80 were conducted: binary mixture of toluene and EA (Fig. 6a); toluene and EtSH (Fig. 6b); EA and EtSH (Fig. 6c) and ternary mixture of toluene, EA and EtSH (Fig. 6d). Fig. 6a reveals that the degradation efficiencies for toluene and EA are beyond 90% within 90 min. Compared with single-compound degradation system (Fig. 5b), it is noted that the photocatalytic oxidation efficiencies for single and binary system are very close, although the former is slightly higher than the latter. Similar conclusion was also obtained for the photocatalytic degradation of the mixtures of toluene and ethyl benzene, suggesting that this was due to the small interference effect among tested VOCs within the selected concentration range [39]. This interference effect was also found in the photocatalytic oxidation of mixed toluene and benzene [40] and during the combustion oxidation of benzene–EA mixtures [41]. Moreover, Lichtin et al. [42] also observed the inhibition effect on the removal efficiencies of single compound by the

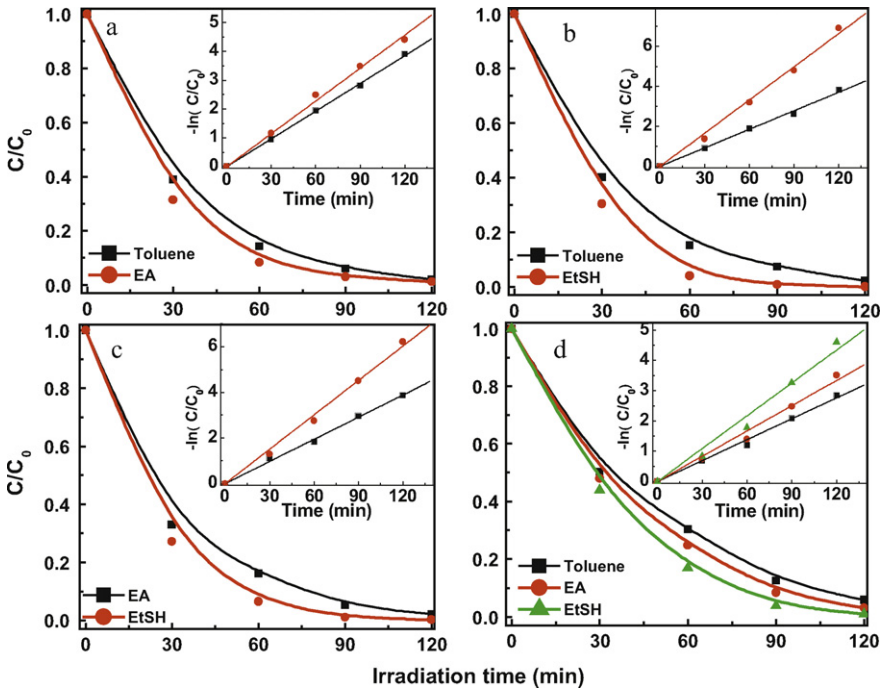

Fig. 6. Photocatalytic degradation kinetics of toluene with EA (a), toluene with EtSH (b), EA with EtSH (c) and toluene, EA with EtSH (d) onto CTMS80.

other component after they tested 14 binary mixtures of VOCs. They explained that the inhibition may be a consequence of competition reaction onto the catalyst. Therefore, the conclusion can be made here that weak mutual inhibition appears to occur in the photocatalytic oxidation of mixed toluene and EA due to the competitive adsorption of reactants on the photocatalyst, leading to the slight decrease of degradation efficiencies for the binary system. The decrease of photocatalytic oxidation efficiencies are also observed in other competitive degradation experiments exhibited in Fig. 6b–d, respectively. It is worth mentioning that for ternary-component degradation, the degradation efficiencies of toluene, EA and EtSH are all beyond 94% within 120 min, further confirming that CTMS80 is an excellent photocatalyst and the mutual inhibition is very slight.

Moreover, L–H model is also applied to fit the photocatalytic degradation kinetics of mixed toluene, EA and EtSH of different component on CTMS80, and the linear plots of $-\ln(C/C_0)$ versus the irradiation time inserted in Fig. 6 and Fig. S3 show that all data well follow the L–H model. The relative reaction rate constants are summarized in Table 2. For toluene in binary-component photocatalytic degradation with EA (or EtSH), the reaction rate constant is 0.0321 min^{-1} (or 0.0309 min^{-1}) which is lower than that in single toluene degradation (0.0338 min^{-1}) and continues to decrease to 0.0230 min^{-1} in ternary-component degradation. Similar decreasing tendency of the reaction rate constants for EA or EtSH from single-component, binary-component to ternary-component degradation can be also obtained (insets in Fig. S3). Apparently, rate constants for degradation of mixed VOCs are lower than that of single component. Such decreasing should be owing to the competitive adsorption occurred before and during the photocatalytic degradation process. As discussed, the photocatalytic degradation rate constants for single model pollutants follow the order of toluene < EA < EtSH. The rate constants of them for binary- and ternary-component degradation also follow the same order. Additionally, the order of the photocatalytic degradation rate constants for model pollutants is consistent with the order of the adsorption ability for them onto CTMS80, which agrees with the previous observation [8] that there was a strong correlation between the degradation rates and the adsorbed concentration of the organic pollutant onto the surface. By analyzing all the results in Table 2, a specific relation between the adsorption capacity and the rate constant is established, that is, for different pollutants of various components, the higher the adsorption capacity is, the greater the photocatalytic reaction rate constant is. The photocatalytic degradation of single or multinary VOCs onto prepared CTMS80 photocatalyst is controlled by the adsorption capability in this system.

4. Conclusions

In the present work, a series of adsorptive CTMS photocatalysts were prepared and applied in purification of single and multinary VOCs from air. Results showed that the prepared composite photocatalysts had excellent adsorption and photocatalytic degradation abilities to three model VOCs. The adsorption capacities of them on these photocatalysts increased in the following order: toluene < EA < EtSH, and the isothermal adsorption data were well described by Langmuir isotherm model compared to Freundlich model. Competitive adsorption resulted in the decrease in the adsorption capacities as well as the photocatalytic degradation efficiencies in multi-component VOCs systems. All photocatalytic degradation kinetics followed the L–H model regardless of single or multinary VOCs system. The reaction rate constants for photocatalytic degradation of mixed VOCs system were all lower than those counterparts in single VOCs system, which followed the order of toluene < EA < EtSH. Thus, a convincing conclusion can be drawn that the higher the adsorption capacity was, the greater the photocatalytic reaction rate constant was for different pollutants of various components.

Acknowledgements

This is contribution No. IS–1324 from GIGCAS. This work was financially supported by Science and Technology Project of Guangdong Province, China (2007A032301002, 2009B030400001, 2009A030902003 and 2006A36701002) and NSFC (40572173).

Appendix A. Supplementary data

Supplementary data associated with this article can be found, in the online version, at doi:10.1016/j.jhazmat.2011.03.064.

References

[1] R.M. Alberici, W.E. Jardim, Photocatalytic destruction of VOCs in the gas-phase using titanium dioxide, Appl. Catal. B-Environ. 14 (1997) 55–68.
[2] R. Beauchet, P. Magnoux, J. Mijoin, Catalytic oxidation of volatile organic compounds (VOCs) mixture (isopropanol/o-xylene) on zeolite catalysts, Catal. Today 124 (2007) 118–123.
[3] H. Jorio, K. Kiared, R. Brzezinski, A. Leroux, G. Viel, M. Heitz, Treatment of air polluted with high concentrations of toluene and xylene in a pilot-scale biofilter, J. Chem. Technol. Biotechnol. 73 (1998) 183–196.
[4] L. Sun, G.Y. Li, S.G. Wan, T.C. An, Mechanistic study and mutagenicity assessment of intermediates in photocatalytic degradation of gaseous toluene, Chemosphere 78 (2010) 313–318.
[5] M.L. Zhang, T.C. An, J.M. Fu, G.Y. Sheng, X.M. Wang, X.H. Hu, X.J. Ding, Photocatalytic degradation of mixed gaseous carbonyl compounds at low level on adsorptive TiO_2/SiO_2 photocatalyst using a fluidized bed reactor, Chemosphere 64 (2006) 423–431.
[6] K. Demeestere, J. Dewulf, H. Van Langenhove, Heterogeneous photocatalysis as an advanced oxidation process for the abatement of chlorinated, monocyclic aromatic and sulfurous volatile organic compounds in air: state of the art, Crit. Rev. Environ. Sci. Technol. 37 (2007) 489–538.
[7] T.C. An, M.L. Zhang, X.M. Wang, G.Y. Sheng, J.M. Fu, Photocatalytic degradation of gaseous trichloroethene using immobilized ZnO/SnO_2 coupled oxide in a flow-through photocatalytic reactor, J. Chem. Technol. Biotechnol. 80 (2005) 251–258.
[8] M.R. Hoffmann, S.T. Martin, W.Y. Choi, D.W. Bahnemann, Environmental applications of semiconductor photocatalysis, Chem. Rev. 95 (1995) 69–96.
[9] J. Matos, J. Laine, J.M. Herrmann, Synergy effect in the photocatalytic degradation of phenol on a suspended mixture of titania and activated carbon, Appl. Catal. B-Environ. 18 (1998) 281–291.
[10] J. Matos, J. Laine, J.M. Herrmann, Association of activated carbons of different origins with titania in the photocatalytic purification of water, Carbon 37 (1999) 1870–1872.
[11] M. Harper, C.J. Purnell, Alkylammonium montmorillonites as adsorbents for organic vapors from air, Environ. Sci. Technol. 24 (1990) 55–62.
[12] L.Z. Zhu, B.L. Chen, S. Tao, C.T. Chiou, Interactions of organic contaminants with mineral-adsorbed surfactants, Environ. Sci. Technol. 37 (2003) 4001–4006.
[13] H. Yoneyama, S. Haga, S. Yamanaka, Photocatalytic activities of microcrystalline TiO_2 incorporated in sheet silicates of clay, J. Phys. Chem. 93 (1989) 4833–4837.
[14] T. Endo, M.M. Mortland, T.J. Pinnavaia, Intercalation of silica in smectite, Clay. Clay Miner. 28 (1980) 105–110.
[15] X.J. Ding, T.C. An, G.Y. Li, J.X. Chen, G.Y. Sheng, J.M. Fu, J.C. Zhao, Photocatalytic degradation of dimethyl phthalate ester using novel hydrophobic TiO_2 pillared montmorillonite photocatalyst, Res. Chem. Intermediat. 34 (2008) 67–83.
[16] M. Lim, Y. Zhou, B. Wood, L.Z. Wang, V. Rudolph, G.Q. Lu, Highly thermostable anatase titania-pillared clay for the photocatalytic degradation of airborne styrene, Environ. Sci. Technol. 43 (2009) 538–543.
[17] C. Ooka, H. Yoshida, K. Suzuki, T. Hattori, Adsorption and photocatalytic degradation of toluene vapor in air on highly hydrophobic TiO_2 pillared clay, Chem. Lett. 32 (2003) 896–897.
[18] J.F. Tanguay, S.L. Suib, R.W. Coughlin, Dichloromethane photodegradation using titanium catalysts, J. Catal. 117 (1989) 335–347.
[19] Z. Ding, H.Y. Zhu, P.F. Greenfield, G.Q. Lu, Characterization of pore structure and coordination of titanium in TiO_2 and SiO_2–TiO_2 sol-pillared clays, J. Colloid Interface Sci. 238 (2001) 267–272.
[20] H.Y. Zhu, J.Y. Li, J.C. Zhao, G.J. Churchman, Photocatalysts prepared from layered clays and titanium hydrate for degradation of organic pollutants in water, Appl. Clay Sci. 28 (2005) 79–88.
[21] D.S. Bhatkhande, V.G. Pangarkar, A.A.C.M. Beenackers, Photocatalytic degradation for environmental applications – a review, J. Chem. Technol. Biotechnol. 77 (2002) 102–116.
[22] Y. Kuwahara, K. Maki, Y. Matsumura, T. Kamegawa, K. Mori, H. Yamashita, Hydrophobic modification of a mesoporous silica surface using a fluorine-containing silylation agent and its application as an advantageous host material for the TiO_2 photocatalyst, J. Phys. Chem. C. 113 (2009) 1552–1559.
[23] C. Ooka, H. Yoshida, M. Horio, K. Suzuki, T. Hattori, Adsorptive and photocatalytic performance of TiO_2 pillared montmorillonite in degradation of endocrine disruptors having different hydrophobicity, Appl. Catal. B-Environ. 41 (2003) 313–321.
[24] C. Ooka, H. Yoshida, K. Suzuki, T. Hattori, Effect of surface hydrophobicity of TiO_2-pillared clay on adsorption and photocatalysis of gaseous molecules in air, Appl. Catal. A-Gen. 260 (2004) 47–53.
[25] K. Shimizu, H. Murayama, A. Nagai, A. Shimada, T. Hatamachi, T. Kodama, Y. Kitayama, Degradation of hydrophobic organic pollutants by titania pillared fluorine mica as a substrate specific photocatalyst, Appl. Catal. B-Environ. 55 (2005) 141–148.
[26] Y.H. Liu, X. Quan, Y.M. Sun, J.W. Chen, D.M. Xue, J.S. Chung, Simultaneous removal of ethyl acetate and toluene in air streams using compost-based biofilters, J. Hazard. Mater. 95 (2002) 199–213.
[27] A.V. Vorontsov, E.V. Savinov, L. Davydov, P.G. Smirniotis, Photocatalytic destruction of gaseous diethyl sulfide over TiO_2, Appl. Catal. B-Environ. 32 (2001) 11–24.
[28] J.Y. Chen, X.L. Liu, G.Y. Li, X. Nie, T.C. An, S.Q. Zhang, H.J. Zhao, Synthesis and characterization of novel SiO_2 and TiO_2 co-pillared montmorillonite composite for adsorption and photocatalytic degradation of hydrophobic organic pollutants in water, Catal. Today (2010), doi:10.1016/j.cattod.2010.11.014.
[29] T.C. An, J.K. Liu, G.Y. Li, S.Q. Zhang, H.J. Zhao, X.Y. Zeng, G.Y. Sheng, J.M. Fu, Structural and photocatalytic degradation characteristics of hydrothermally treated mesoporous TiO_2, Appl. Catal. A-Gen. 350 (2008) 237–243.
[30] M. Kruk, M. Jaroniec, Gas adsorption characterization of ordered organic–inorganic nanocomposite materials, Chem. Mater. 13 (2001) 3169–3183.
[31] S.W. Lee, H.J. Park, S.H. Lee, M.G. Lee, Comparison of adsorption characteristics according to polarity difference of acetone vapor and toluene vapor on silica–alumina fixed-bed reactor, J. Ind. Eng. Chem. 14 (2008) 10–17.
[32] F.A. Banat, B. Al-Bashir, S. Al-Asheh, O. Hayajneh, Adsorption of phenol by bentonite, Environ. Pollut. 107 (2000) 391–398.
[33] A. Ozer, D. Ozer, H.I. Ekiz, Application of Freundlich and Langmuir models to multistage purification process to remove heavy metal ions by using *Schizomeris leibleinii*, Process Biochem. 34 (1999) 919–927.
[34] S. Rengaraj, J.W. Yeon, Y. Kim, Y. Jung, Y.K. Ha, W.H. Kim, Adsorption characteristics of Cu(II) onto ion exchange resins 252H and 1500H: kinetics, isotherms and error analysis, J. Hazard. Mater. 143 (2007) 469–477.
[35] S.W. Lee, J.K. Cheon, H.J. Park, M.G. Lee, Adsorption characteristics of binary vapors among acetone, MEK, benzene, and toluene, Korean J. Chem. Eng. 25 (2008) 1154–1159.
[36] J. Wyman, Polarization and dielectric constant of liquids, J. Am. Chem. Soc. 58 (1936) 1482–1486.
[37] R. Yang, Y.P. Zhang, Q.J. Xu, J.H. Mo, R.Y. Zhao, Experimental study on the photocatalytic oxidation of mixed toluene and benzene, in: Indoor Air 2005: Proceedings of the 10th International Conference on Indoor Air Quality and Climate, vol. 1–5, 2005, pp. 3041–3045.
[38] T.C. An, L. Sun, G.Y. Li, S.G. Wan, Gas-phase photocatalytic degradation and detoxification of o-toluidine: degradation mechanism and Salmonella mutagenicity assessment of mixed gaseous intermediates, J. Mole. Catal. A: Chem. 333 (2010) 128–135.
[39] W. Chen, J.S. Zhang, UV-PCO device for indoor VOCs removal: investigation on multiple compounds effect, Build. Environ. 43 (2008) 246–252.
[40] Y.P. Zhang, R. Yang, Q.J. Xu, J.H. Mo, Characteristics of photocatalytic oxidation of toluene, benzene, and their mixture, J. Air Waste Manage. Assoc. 57 (2007) 94–101.
[41] P. Papaefthimiou, T. Ioannides, X.E. Verykios, Performance of doped Pt/TiO_2 (W^{6+}) catalysts for combustion of volatile organic compounds (VOCs), Appl. Catal. B-Environ. 15 (1998) 75–92.
[42] N.N. Lichtin, M. Avudaithai, E. Berman, A. Grayfer, TiO_2-photocatalyzed oxidative degradation of binary mixtures of vaporized organic compounds, Sol. Energy 56 (1996) 377–385.